
Multi-Scale VMamba: Hierarchy in Hierarchy Visual State Space Model

Yuheng Shi
City University of Hong Kong
yuhengshi99@gmail.com

Minjing Dong
City University of Hong Kong
minjdong@cityu.edu.hk

Chang Xu
University of Sydney
c.xu@sydney.edu.au

Abstract

Despite the significant achievements of Vision Transformers (ViTs) in various vision tasks, they are constrained by the quadratic complexity. Recently, State Space Models (SSMs) have garnered widespread attention due to their global receptive field and linear complexity with respect to the input length, demonstrating substantial potential across fields including natural language processing and computer vision. To improve the performance of SSMs in vision tasks, a multi-scan strategy is widely adopted, which leads to significant redundancy of SSMs. For a better trade-off between efficiency and performance, we analyze the underlying reasons behind the success of the multi-scan strategy, where long-range dependency plays an important role. Based on the analysis, we introduce Multi-Scale Vision Mamba (MSVMamba) to preserve the superiority of SSMs in vision tasks with limited parameters. It employs a multi-scale 2D scanning technique on both original and downsampled feature maps, which not only benefits long-range dependency learning but also reduces computational costs. Additionally, we integrate a Convolutional Feed-Forward Network (ConvFFN) to address the lack of channel mixing. Our experiments demonstrate that MSVMamba is highly competitive, with the MSVMamba-Tiny model achieving 82.8% top-1 accuracy on ImageNet, 46.9% box mAP, and 42.2% instance mAP with the Mask R-CNN framework, 1x training schedule on COCO, and 47.6% mIoU with single-scale testing on ADE20K. Code is available at <https://github.com/YuHengsss/MSVMamba>.

1 Introduction

In the domain of computer vision, the extraction of features plays a pivotal role in the performance of various tasks, ranging from image classification to more complex applications like detection and segmentation. Traditionally, Convolutional Neural Networks (CNNs) [26, 41, 19, 22, 34] have been the backbone of feature extraction methodologies, prized for their linear scaling complexity and proficiency in capturing local patterns. However, CNNs often fall short in encapsulating global context, a limitation that becomes increasingly apparent in tasks requiring a comprehensive understanding of the entire visual field. In contrast, Vision Transformers (ViTs) [6, 33, 51, 44] have emerged as a compelling alternative, boasting an inherent global receptive field that allows for the direct capture of long-range dependencies within an image. Despite their advantages, ViTs are hampered by their quadratic scaling complexity concerning the input size, which significantly constrains their applicability to downstream tasks such as object detection and segmentation, where efficiency is paramount. Recently, State Space Model (SSM)-based approaches [12, 42, 8] have garnered attention for their ability to combine the best of both worlds: a global receptive field and linear scaling complexity. Notably, Mamba [10] introduces a hardware-aware and input-dependent algorithm that significantly enhances the performance and efficiency of SSMs. Inspired by Mamba's success, a burgeoning body of work has sought to leverage its advantages for vision tasks, pioneering efforts such as ViM [61] and VMamba [31].

The S6 block, developed by Mamba [10], was originally designed for NLP tasks. To adapt S6 for vision tasks, images are first divided into patches and then flattened into a patch sequence along the scanning path. To accommodate the non-causal nature of image data, the multi-scan strategy is widely adopted for vision tasks, such as ViM [61] which enhances the sequence by summing it in both forward and reverse directions, and VMamba [31] which integrates horizontal and vertical scans. However, unlike NLP models, which can have up to billions of parameters, current vision backbones always take computational costs into consideration, *i.e.*, the trade-off between accuracy and efficiency. This constraint on model size inherently limits the long-range modeling capabilities of SSMs in vision tasks. Taking ViM-Tiny [61] as an example, placing the cls token in the middle of the sequence yields markedly better results than positioning it at the ends. This suggests that central placement compensates for the model’s limited ability to integrate distant information, highlighting the difficulties of handling long-range dependencies in parameter-constrained vision models. We refer to this as the long-range forgetting problem. In this work, we analyze how the multi-scan strategy in [61, 31] helps to alleviate this problem. Compared to the single-scan strategy, the multi-scan one allows long-range decay to manifest in various directions within 2D images. However, the increased scanning routes bring multiples of computations, significantly increasing redundancy and limiting efficiency. Thus, we aim to pursue a better trade-off between the performance and efficiency of Mamba in vision tasks.

The most direct and effective method to address the long-range forgetting problem is to shorten the sequence length, which can be achieved by downsampling the feature map. However, placing all scanning routes on a downsampled feature map could result in the loss of fine-grained features and the downstream task performance. Through the visualization of different scans, we show that the decay rates could vary for different scanning routes, which motivates us to develop a hierarchical design of multi-scan. In this work, we propose a Multi-Scale 2D (MS2D) scanning strategy to alleviate the long-range forgetting problem with limited computational costs. Specifically, we divide the scanning directions of SS2D [31] into two groups: one retains the original resolution and is processed by the S6 block, while the others are downsampled, processed by the S6 block, and then upsampled, which not only shortens the sequence length for long-range dependencies learning but also alleviates redundancy. Building on the VMamba with its hierarchical architecture, we incorporate another hierarchical design within the block, creating a hierarchy within a hierarchy. Furthermore, we introduce a Convolutional Feed-Forward Network (ConvFFN) within each block to bolster the model’s capability for channel-wise information exchange and local feature capture.

We conduct extensive experiments to validate the effectiveness of MSVMamba across a spectrum of tasks, including image classification, object detection, and semantic segmentation. Detailed comparisons on the ImageNet-1K [3] dataset are illustrated in Fig. 1. Specifically, MSVMamba-Tiny achieves a notable improvement over VMamba-Tiny, enhancing the Top-1 accuracy by 0.6% while concurrently reducing the computational demand by 17% in terms of GFLOPs. Furthermore, our MSVMamba model also surpasses SOTA SSM-based models in performance on the COCO [29] and ADE20K [59] datasets for object detection and semantic segmentation tasks, respectively.

2 Related work

2.1 Generic Vision Backbone

The evolution of generic vision backbones has significantly shaped the landscape of computer vision, transitioning from CNNs [26, 41, 19, 55, 22, 20, 43, 34] to ViTs [6, 33, 32, 51, 52, 5, 44, 58]. CNNs have been the cornerstone of vision-based models, dominating vision tasks in the early era of deep learning. The classic CNNs such as AlexNet [26], VGG [41], and ResNet [19], have paved the way for numerous subsequent innovations [55, 22, 20, 43, 21, 34, 4, 50]. These designs have significantly improved performance on a wide range of vision tasks by enhancing the network’s ability to capture

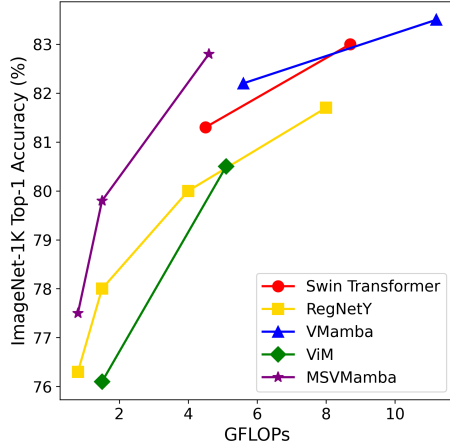


Figure 1: Comparison on ImageNet.

complex patterns and features from visual data. The Vision Transformer [6], drawing inspiration from the success of transformers [48] in natural language processing, has emerged as a formidable contender to conventional CNNs for vision-related tasks. ViT reimagines image processing by segmenting an image into patches and employing self-attention mechanisms to process these segments. This innovative approach enables the model to discern global dependencies across the entire image, a significant leap forward in understanding complex visual data. However, the ViT architecture demands considerable computational resources and extensive datasets for effective training. Moreover, its performance is intricately tied to the input sequence length, exhibiting a quadratic complexity that can escalate processing costs. In response, subsequent research has focused on developing more efficient training strategies [44, 46, 25], hierarchical network structures [33, 32, 5, 51, 52, 16], refined spatial attention mechanisms [58, 60, 53, 47, 17, 5] and convolution-based design [2, 30, 15, 37] to address these issues.

2.2 State Space Models

State Space Models (SSMs) [11, 13, 12, 42, 8] have garnered increasing attention from researchers due to their computational complexity, which grows linearly with the length of the input sequence, and their inherent global awareness properties. To reduce the computational resource consumption of SSMs, S4 [12] introduced a diagonal structure and combined it with a diagonal plus low-rank approach to construct structured SSMs. Subsequently, S5 [42] and H3 [8] further enhanced the efficiency of SSM-based models by introducing parallel scanning techniques and improving hardware utilization. Mamba [10] then introduced the S6 block, incorporating data-dependent parameters to amend the Linear Time Invariant(LTI) characteristics of previous SSM models, demonstrating superior performance over transformers on large-scale datasets. In the realm of vision tasks, S4ND [36] pioneered the application of SSM models in vision tasks by treating visual data as 1D, 2D, and 3D signals. U-Mamba [35] combined CNNs with SSMs for medical image segmentation. ViM [61] and VMamba [31] integrated the S6 block into vision backbone design, employing multiple scanning directions to accommodate the non-casual nature of image data, achieving competitive results against ViTs and CNNs. Motivated by the success of ViM and VMamba, a plethora of Mamba-based works [38, 24, 7, 56, 1, 27, 57, 40] have emerged across various vision tasks, including vision backbone design [38, 24, 56], medical image segmentation [40, 28], and video classification [27], showcasing the potential of SSM-based approaches in advancing the field of computer vision.

3 Method

In this section, we first summarize the state space model in Section 3.1. Subsequently, in Section 3.2, we provide an in-depth analysis of the multi-scan strategy in existing vision Mamba models. Following the analysis, Section 3.3 tackles the redundancy and long-range dependency issue by introducing a Multi-Scale 2D (MS2D) scanning strategy. Finally, Section 3.4 details the integration of the Multi-Scale State Space (MS3) block, which incorporates the MS2D technique alongside a ConvFFN. Building upon the MS3 block, various model configurations are developed across different scales, illustrating the adaptability and scalability of our proposed approach.

3.1 Preliminaries

State Space Models. Classical State Space Models (SSMs) represent a continuous system that maps an input sequence $x(t) \in \mathbb{R}^L$ to a latent space representation $h(t) \in \mathbb{R}^N$ and subsequently predicts an output sequence $y(t) \in \mathbb{R}^L$ based on this representation. Mathematically, an SSM can be described as follows:

$$h'(t) = \mathbf{A}h(t) + \mathbf{B}x(t), \quad y(t) = \mathbf{C}h(t), \quad (1)$$

where $\mathbf{A} \in \mathbb{R}^{N \times N}$, $\mathbf{B} \in \mathbb{R}^{N \times 1}$ and $\mathbf{C} \in \mathbb{R}^{1 \times N}$ are learnable parameters.

Discretization. To adapt continuous State Space Models (SSMs) for use within deep learning frameworks, it is crucial to implement discretization operations. By incorporating a timescale parameter $\Delta \in \mathbb{R}$ and employing the widely utilized zero-order hold (ZOH) as the discretization rule, the discretized versions of \mathbf{A} and \mathbf{B} (denoted as $\bar{\mathbf{A}}$ and $\bar{\mathbf{B}}$, respectively) can be derived, with which,

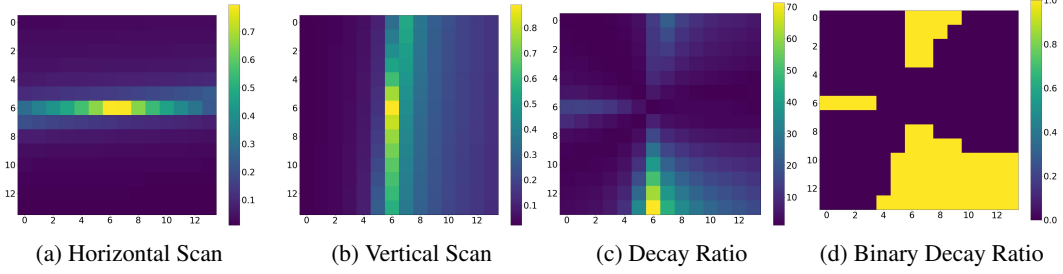


Figure 2: Illustration of decay along horizontal, vertical scanning routes and their ratio.

Eq. 1 can be reformulated into a discretized manner as:

$$h(t) = \bar{\mathbf{A}}h(t-1) + \bar{\mathbf{B}}x(t), \quad y(t) = \mathbf{C}h(t),$$

$$\text{where } \bar{\mathbf{A}} = e^{\Delta\mathbf{A}}, \quad \bar{\mathbf{B}} = (\Delta\mathbf{A})^{-1}(e^{\Delta\mathbf{A}} - \mathbf{I})\Delta\mathbf{B} \approx \Delta\mathbf{B}, \quad (2)$$

where \mathbf{I} denotes the identity matrix. Afterward, the process of Eq. 2 could be implemented in a global convolution manner as:

$$y = x \odot \bar{\mathbf{K}}, \quad \bar{\mathbf{K}} = \left(\mathbf{C}\bar{\mathbf{B}}, \mathbf{C}\bar{\mathbf{A}}\bar{\mathbf{B}}, \dots, \mathbf{C}\bar{\mathbf{A}}^{L-1}\bar{\mathbf{B}} \right), \quad (3)$$

where $\bar{\mathbf{K}} \in \mathbb{R}^L$ is the convolution kernel.

Selective State Space Models. The Selective State Space (S6) mechanism, introduced by Mamba [10], renders the parameters $\bar{\mathbf{B}}, \bar{\mathbf{C}},$ and Δ input-dependent, thereby enhancing the performance of SSM-based models. After making $\bar{\mathbf{B}}, \bar{\mathbf{C}},$ and Δ input-dependent, the global convolution kernel in Eq. 3 could be rewritten as:

$$\bar{\mathbf{K}} = \left(\mathbf{C}_L\bar{\mathbf{B}}_L, \mathbf{C}_L\bar{\mathbf{A}}_{L-1}\bar{\mathbf{B}}_{L-1}, \dots, \mathbf{C}_L \prod_{i=1}^{L-1} \bar{\mathbf{A}}_i\bar{\mathbf{B}}_1 \right). \quad (4)$$

3.2 Analysis of Multi-Scan Strategy

When processing image data using the S6 block, the 2D feature map $\mathbf{Z} \in \mathbb{R}^{H \times W \times D}$ is flattened into a 1D sequence of image tokens, denoted as $\mathbf{X} \in \mathbb{R}^{L \times D}$. According to Eq. 4 and Eq. 2, the contribution of the m_{th} token to the construction of the n_{th} token ($m < n$) in S6 can be expressed as:

$$\mathbf{C}_n \prod_{i=m}^n \bar{\mathbf{A}}_i \bar{\mathbf{B}}_m = \mathbf{C}_n \bar{\mathbf{A}}_{(m \rightarrow n)} \bar{\mathbf{B}}_m, \quad \text{where } \bar{\mathbf{A}}_{(m \rightarrow n)} = e^{\sum_{i=m}^n \Delta_i \mathbf{A}}. \quad (5)$$

Typically, the learned $\Delta_i \mathbf{A}$ is negative, which biases the model towards prioritizing recent tokens' information. Consequently, as the sequence length increases, the exponential term $e^{\sum_{i=m}^n \Delta_i \mathbf{A}}$ in Eq. 5 decays significantly, resulting in minimal contributions from distant tokens. We refer to it as the long-range forgetting issue, which has also been observed in recent studies applying S6 to vision tasks [14]. Although this problem can be mitigated by increasing the number of parameters and the depth of the model, such adjustments introduce additional computational costs. Furthermore, the causal property of the S6 block ensures that information can only propagate in a unidirectional manner between tokens, preventing earlier tokens from accessing information from subsequent tokens.

The inherent non-causal nature of images renders the direct application of the S6 block to vision-related tasks less than optimal, as identified by ViM [61]. To mitigate this limitation, ViM [61] and VMamba [31] have introduced methodologies that entail scanning image features across various directions and then integrating these features. Generally, the updated token along one of the scanning routes, denoted as $Scan(\mathbf{Z}_{(p,q)})$, where (p, q) indicates the coordinate, could be obtained by:

$$Scan(\mathbf{Z}_{(p,q)}) = \mathbf{C}_\alpha \sum_{i=1}^{\alpha} \bar{\mathbf{A}}_{(i \rightarrow \alpha)} \bar{\mathbf{B}}_i \sigma(\mathbf{Z})_i. \quad (6)$$

In Eq. 6, σ represents the transformation that converts a 2D feature map into a 1D sequence, and α denotes the corresponding index of $\mathbf{Z}_{(p,q)}$ in the transformed 1D sequence. Afterward, results from multi-scan routes are added together to produce enhanced feature $\mathbf{Z}'(p, q)$, which can be denoted as:

$$\mathbf{Z}'_{(p,q)} = \sum_k Scan_k(\mathbf{Z}_{(p,q)}) = \sum_k \mathbf{C}_{\alpha_k} \sum_{i=1}^{\alpha_k} \bar{\mathbf{A}}_{(i \rightarrow \alpha_k)} \bar{\mathbf{B}}_i \sigma_k(\mathbf{Z})_i. \quad (7)$$

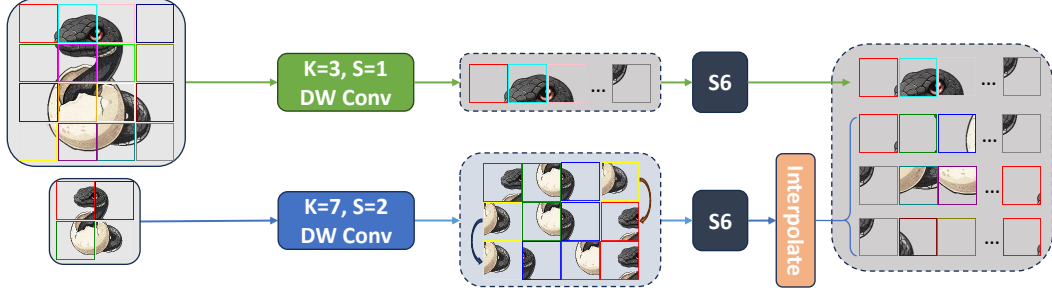


Figure 3: Illustration of the Multi-Scale 2D-Selective-Scan on an image

This multi-scan strategy allows tokens to access information from each other. In ViM [61], two distinct scanning routes correspond to two different transformations in Eq. 6, specifically, the flatten and the flatten with flip transformations. Similarly, VMamba [31] extends the basic bidirectional scanning by incorporating both horizontal and vertical scanning directions, yielding four distinct scanning routes. Besides, the multi-scan strategy also alleviates the long-range forgetting problem by minimizing the effective distance between tokens. For tokens at coordinates (p_1, q_1) and (p_2, q_2) , the strategy employs multiple scanning routes, each potentially altering their relative positions. The minimum distance across these routes is given by $\min_k d_k((p_1, q_1) \rightarrow (p_2, q_2))$, where d_k represents the distance between the tokens in the sequence generated by the k -th scan. By reducing this distance, the multi-scan strategy reduces the decay of influence between distant tokens, thereby enhancing the model’s ability to maintain and utilize long-range information.

To more intuitively demonstrate the relationship between the multi-scan strategy and long-range decay, we visualize the exponential term $e^{\sum_{i=1}^{\alpha} \Delta_i \mathbf{A}}$ along the horizontal and vertical scanning directions in VMamba-Tiny with respect to the central token in Fig. 2a and Fig. 2b. Specifically, we randomly select 50 images from the ImageNet [3] validation set and compute the average decay along scanning routes at the last layer of the final stage across these images and feature dimensions. We use a higher input resolution to enhance the quality of the visualization.

According to these observations, the success of the multi-scan strategy in VMamba can be attributed to its mitigation of the non-causal properties of image data and alleviation of the long-range forgetting problem. However, as the number of scanning routes increases, the computational cost also rises linearly, introducing computational redundancy. In Fig. 2c, we illustrate the maximum ratio of Fig. 2a to Fig. 2b and vice versa. While in Fig. 2d, we present a binarized version of Fig. 2c, applying a threshold of 10, which covers more than 40% of the entire figure. This phenomenon indicates that the varying decay rates across different scanning routes lead to certain routes dominating the decay dynamics, which can also be attributed to the long-range forgetting problem. The existence of dominant scanning routes implies that some scans contribute significantly more to information retention than others, leading to computational redundancy in the multi-scan strategy.

3.3 Multi-Scale 2D Scanning

As discussed in the last subsection, the contribution of tokens decays with increasing scanning distance. The most effective and direct way to alleviate the long-range forgetting problem is to reduce the number of tokens. Simultaneously, since the computational complexity of the S6 block is linearly dependent on the number of tokens, reducing the token count also enhances efficiency. Thus, an alternative approach to address the aforementioned issue is to apply the multi-scan strategy on a downsampled feature map. However, setting all scans on a downsampled feature map will ignore fine-grained features and result in unavoidable information loss. Thus, scanning along the full-resolution feature map is also essential.

Motivated by these considerations, we introduce a simple yet effective Multi-Scale 2D scanning (MS2D) strategy, as depicted in Fig. 3. Our approach commences with the generation of hierarchical feature maps at varying scales, achieved through the application of Depthwise Convolution (DWConv) with distinct stride values. These multi-scale feature maps are then processed through four distinct scanning routes within VMamba. Specifically, we utilize DWConvs with strides of 1 and s to obtain feature map $\mathbf{Z}_1 \in \mathbb{R}^{H \times W \times D}$ and $\mathbf{Z}_2 \in \mathbb{R}^{\frac{H}{s} \times \frac{W}{s} \times D}$, respectively. Afterwards, \mathbf{Z}_1 and

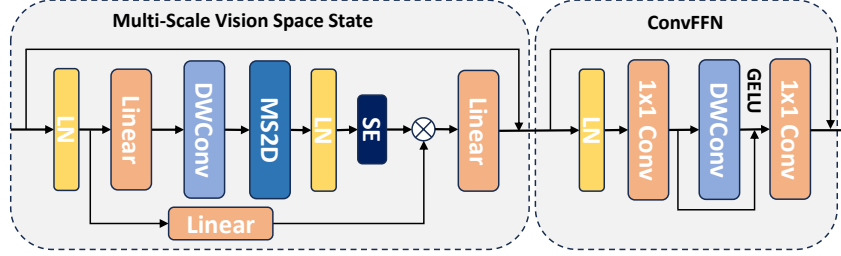


Figure 5: Detailed architecture of Multi-Scale State Space (MS3) block, consisting of a Multi-Scale Vision Space State (MSVSS) block and a Convolutional Feed-Forward Network (ConvFFN) block.

\mathbf{Z}_2 are processed by two S6 blocks as:

$$\mathbf{Y}_1 = S6(\sigma_1(\mathbf{Z}_1)), \quad (8)$$

$$[\mathbf{Y}_2, \mathbf{Y}_3, \mathbf{Y}_4] = S6([\sigma_2(\mathbf{Z}_2), \sigma_3(\mathbf{Z}_2), \sigma_4(\mathbf{Z}_2)]), \quad (9)$$

where σ is transformation that convert 2D feature maps into 1D sequences used in SS2D, and \mathbf{Y} is the processed sequence. These processed sequences are converted back into 2D feature maps, and the downsampled feature maps are interpolated for merging:

$$\mathbf{Z}'_i = \gamma_i(\mathbf{Y}_i), i \in \{1, 2, 3, 4\}, \quad (10)$$

$$\mathbf{Z}' = \mathbf{Z}'_1 + \text{Interpolate}(\sum(\mathbf{Z}'_j)), j \in \{2, 3, 4\}, \quad (11)$$

where γ is the inverse transformation of σ and \mathbf{Z}' is the feature map enhanced by MS2D.

The downsampling operation reduces the sequence length by a factor of s^2 , which also shortens the distance between tokens in Eq. 5 by a factor of s^2 , thereby alleviating the long-range forgetting problem. As the computational complexity of a single S6 block is $O(9LDN)$ [10], where N denotes the SSM dimension, replacing SS2D with MS2D reduces the total sequence length across four scans from $4L$ to $(1+3/s^2)L$, thereby improves the efficiency. Practically, the downsampling rate is set to 2. It is worth noting that sequences from \mathbf{Z}_2 are processed by the same S6 block. This approach maintains the same accuracy as using multiple S6 blocks for different scanning routes while effectively reducing the number of parameters.

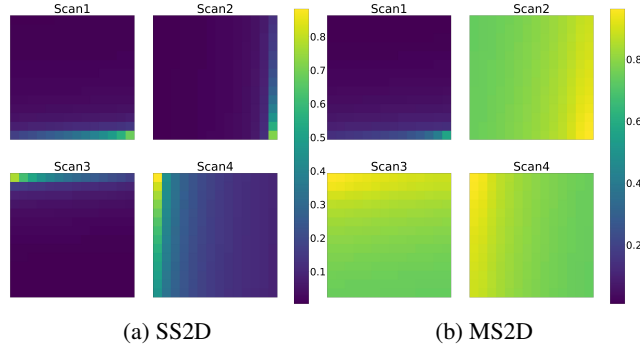


Figure 4: Illustration of the decay with different scanning routes in SS2D and MS2D.

To better illustrate the alleviation of the long-range forgetting problem, we also provide empirical evidence, as shown in Fig. 4. We compare the decay along scanning routes in the SS2D of VMamba and our MS2D, focusing on the last token with the same configuration as Fig. 2. The decay maps in downsampled features are interpolated back. As observed, the decay rate along scanning routes in downsampled maps is significantly alleviated, enhancing the capability to capture global information.

3.4 Overall Model Architecture

In this study, we extend the capabilities of the VMamba framework by substituting its VSS block with our Multi-Scale State Space (MS3) block. The architectural framework of the MS3 block is delineated in Fig. 5, comprising a Multi-Scale Vision Space State (MSVSS) component and a Convolutional Feed-Forward Network (ConvFFN). The MSVSS component is devised by adapting the vision state space framework in VMamba, substituting the SS2D with an MS2D to further introduce a hierarchy design in a single layer. Additionally, a Squeeze-Excitation (SE) [21] block is integrated subsequent to the multi-scale 2D scanning, as informed by related literature [24, 38]. Diverging from the conventional focus on token mixing in prior vision Mamba architectures [61, 31, 24], our

design introduces a channel mixer to augment the flow of information across different channels, aligning with the structural paradigms of typical vision transformers. In concordance with preceding studies [53, 49, 15, 52], the ConvFFN which consists of a depth-wise convolution and two fully connected layers is employed as the channel mixer. To ensure that the ConvFFN and MSVSS block consume approximately the same FLOPs following LeViT [9], we adopt a modest channel expansion ratio of 2. Upon the amalgamation of MSVSS and ConvFFN within the MS3 block, meticulous adjustments are made to the number of blocks to ensure a comparable computational budget, facilitating a fair comparison.

To empirically validate the efficacy of our proposed modifications, we introduce model variants across different scales, the specifications of which are detailed in our appendix 6. These variants, namely Nano, Micro, and Tiny, are characterized by their parameter counts of 6.9M, 11.9M, and 33.0M, respectively. In terms of computational expenditure, these models require 0.9, 1.5, and 4.6 GFLOPs correspondingly, demonstrating a scalable approach to model design that accommodates varying computational constraints.

4 Experimental Validation

4.1 ImageNet Classification

Settings. Our models are trained and tested on the ImageNet-1K dataset [3]. In alignment with previous works [33, 31, 24], all models undergo training for 300 epochs, with the initial 20 epochs dedicated to warming up. The training utilizes a batch size of 1024 across 8 GPUs. We employ the AdamW optimizer, setting the betas to (0.9, 0.999) and momentum to 0.9. The learning rate is managed through a cosine decay scheduler, starting from an initial rate of 0.001, coupled with a weight decay of 0.05. Additionally, we leverage the exponential moving average (EMA) and implement label smoothing with a factor of 0.1 to enhance model performance and generalization. During testing, images are center cropped with the size of 224×224 . When dealing with the routes for multi-scale scanning, we empirically select top-left to the bottom-right for dealing with the full-resolution feature map while the other three scans are responsible for scanning the downsampled feature map.

Results. Tab. 1 showcases our MSVMamba models against established CNNs, ViTs, and SSM-based models on ImageNet-1K. MSVMamba-N, with 7M parameters and 0.9G FLOPs, achieves 77.3% top-1 accuracy, outperforming similar-cost Conv-based RegNetY-800M and SSM-based EfficientVMamba-T. MSVMamba-M, with 12M parameters and 1.5G FLOPs, reaches 79.8% accuracy, surpassing ViM-T by 3.7%. The MSVMamba-T model attains 82.8% accuracy with 33M parameters and 4.6G FLOPs, exceeding VMamba-T by 0.6% with much less computational cost. These results highlight MSVMamba’s efficiency and scalability, offering a robust option for high-accuracy, resource-efficient model design.

4.2 Object Detection

Setup. We evaluate our MSVMamba on the MSCOCO [29] dataset using the Mask R-CNN [18] framework for object detection and instance segmentation tasks. Following previous works [33, 31],

Table 1: Accuracy comparison across various models on ImageNet-1K.

Method	#param.	FLOPs	Top-1 Acc(%)
RegNetY-800M [39]	6M	0.8G	76.3
RegNetY-1.6G [39]	11M	1.6G	78.0
RegNetY-4G [39]	21M	4.0G	80.0
DeiT-S [44]	22M	4.6G	79.8
DeiT-B [44]	86M	17.5G	81.8
Swin-T [33]	29M	4.5G	81.3
Swin-S [33]	50M	8.7G	83.0
Swin-B [33]	88M	15.4G	83.5
ViM-T [61]	7M	1.5G	76.1
ViM-S [61]	26M	5.1G	80.5
VMamba-T [31]	22M	5.6G	82.2
VMamba-B [31]	44M	11.2G	83.5
LocalVMamba-T [24]	26M	5.7G	82.7
LocalVMamba-S [24]	50M	11.4G	83.7
EffVMamba-T [38]	6M	0.8G	76.5
EffVMamba-S [38]	11M	1.3G	78.7
EffVMamba-B [38]	33M	4.0G	81.8
MSVMamba-N	7M	0.9G	77.3
MSVMamba-M	12M	1.5G	79.8
MSVMamba-T	33M	4.6G	82.8

Table 2: Object detection and instance segmentation with Mask R-CNN on COCO. The FLOPs are computed for an input size of 1280×800 . Multi-scale training is exclusively implemented in the $3 \times$ schedule. All backbones are pre-trained on the ImageNet-1K dataset.

Backbone	Mask R-CNN 1x Schedule						Mask R-CNN 3x Schedule						#param.	FLOPs
	AP ^b	AP ₅₀ ^b	AP ₇₅ ^b	AP ^m	AP ₅₀ ^m	AP ₇₅ ^m	AP ^b	AP ₅₀ ^b	AP ₇₅ ^b	AP ^m	AP ₅₀ ^m	AP ₇₅ ^m		
PVT-T [51]	36.7	59.2	39.3	35.1	56.7	37.3	39.8	62.2	43.0	37.4	59.3	39.9	33M	208G
LightViT-T [23]	37.8	60.7	40.4	35.9	57.8	38.0	41.5	64.4	45.1	38.4	61.2	40.8	28M	187G
EffVMamba-S [38]	39.3	61.8	42.8	36.7	58.9	39.2	41.6	63.9	45.6	38.2	60.8	40.7	31M	197G
MSVMamba-M	43.8	65.8	47.7	39.9	62.9	42.9	46.3	68.1	50.8	41.8	65.1	44.9	32M	201G
Swin-T [33]	42.7	65.2	46.8	39.3	62.2	42.2	46.0	68.1	50.3	41.6	65.1	44.9	48M	267G
ConvNeXt-T [34]	44.2	66.6	48.3	40.1	63.3	42.8	46.2	67.9	50.8	41.7	65.0	44.9	48M	262G
VMamba-T [31]	46.5	68.5	50.7	42.1	65.5	45.3	48.5	69.9	52.9	43.2	66.8	46.3	42M	286G
LocalVMamba-T [24]	46.7	68.7	50.8	42.2	65.7	45.5	48.7	70.1	53.0	43.4	67.0	46.4	45M	291G
EffVMamba-B [38]	43.7	66.2	47.9	40.2	63.3	42.9	45.0	66.9	49.2	40.8	64.1	43.7	53M	252G
MSVMamba-T	46.9	68.8	51.4	42.2	65.6	45.4	48.3	69.5	53.0	43.2	66.8	46.9	53M	252G

we utilize backbones pretrained on ImageNet-1K for initialization. We employ standard training strategies of $1 \times$ (12 epochs) and $3 \times$ (36 epochs) with Multi-Scale (MS) training for a fair comparison.

Results. Tab. 2 presents a performance comparison of our method against CNNs, ViTs, and SSM-based models. Our model consistently outperforms others across various variants and training settings. Specifically, MSVMamba-T outperforms Swin-T by +4.2 box AP and +2.9 mask AP under the $1 \times$ schedule and also shows improvements in both box AP and mask AP under the $3 \times$ schedule.

4.3 Semantic Segmentation

Setup. Consistent with the methodologies used in Swin [33] and VMamba [31], we utilize the UperHead [54] framework atop an ImageNet pre-trained MSVMamba backbone. The training process is conducted over 160K iterations with a batch size of 16. We employ the AdamW optimizer with a learning rate set at 6×10^{-5} . Our experiments are primarily conducted using a default input resolution of 512×512 . Additionally, we also incorporate Multi-Scale (MS) testing to assess performance variations.

Results. We present the detailed results of our model and other competitors in Tab. 3, which includes both single-scale and multi-scale testing. Our MSVMamba consistently outperforms the Swin, ConNeXt, and VMamba models in the tiny variant by margins of +2.2, +1.6, and +0.3 mIoU, respectively.

Table 3: We present the results of semantic segmentation on the ADE20K dataset [59] using the UperNet framework [54]. The computational complexity, measured in FLOPs, is calculated for input dimensions of 512×2048 . The abbreviations "SS" and "MS" refer to single-scale and multi-scale testing, respectively.

Method	mIoU		#param.	FLOPs
	SS	MS		
ResNet-50 [19]	42.1	42.8	67M	953G
DeiT-S+MLN [45]	43.8	45.1	58M	1217G
Swin-T [33]	44.4	45.8	60M	945G
ConvNeXt-T [34]	46.0	46.7	60M	939G
VMamba-T [31]	47.3	48.3	55M	964G
LocalVMamba-T [24]	47.9	49.1	57M	970G
EffVMamba-S [38]	41.5	42.1	29M	505G
EffVMamba-B [38]	46.5	47.3	65M	930G
MSVMamba-M	45.1	45.4	42M	875G
MSVMamba-T	47.6	48.5	65M	942G

4.4 Ablation Study

To validate the effectiveness of the proposed modules, we conducted a comprehensive ablation study. Specifically, we scaled the VMamba-Tiny model by setting its embedding dimension d to 48, the state space dimension N to 8, and the number of blocks in the four different stages to $[1, 2, 4, 2]$. The scaled model, referred to as VMamba-Nano, has parameters and computational costs of 4.4M and 0.87GFLOPs, respectively. This model serves as the baseline for our ablation experiments. Models in ablation study are conducted over a training schedule of 100 epochs, except where noted otherwise, to reduce training time.

On Multi-Scale 2D Scan. After replacing the SS2D in VMamba with our MS2D, while maintaining a roughly equivalent FLOP count, the accuracy increased from 69.6% to 71.9%, as demonstrated in the Tab. 4. Furthermore, we conducted an ablation on the number of scans in the

Table 4: Evolutionary trajectory from VMamba to MSVMamba. When integrating the ConvFFN and setting the state space dimension $N = 1$, we meticulously calibrate the quantity of blocks to maintain a nearly constant computational cost, measured in GFLOPs.

Model	MS2D	SE	ConvFFN	$N = 1$	#param.	FLOPs	Top-1 Acc(%).
VMamba-Nano					4.4M	0.87G	69.6
MSVMamba-Nano	✓				4.8M	0.89G	71.9 \uparrow 2.3
	✓	✓			5.3M	0.89G	72.4 \uparrow 2.8
	✓	✓	✓		6.6M	0.94G	74.4 \uparrow 4.8
	✓	✓	✓	✓	6.9M	0.88G	75.1 \uparrow 5.5

multi-scale scan, considering both full-resolution and half-resolution branches. The results are shown in Tab. 5. Placing all scans in the half-resolution branch led to a significant loss of fine-grained features, resulting in a substantial decrease in model accuracy. Positioning two or three scans in the full resolution branch, compared to just one, resulted in accuracy improvements of 0.1% and 0.6%, respectively, but introduced an additional computational cost of approximately 12% and 25%. Allocating four scans to the full resolution branch, effectively reverting to the SS2D method, increased the computational cost by 34% while only improving accuracy by 0.4%. For an optimal trade-off between computational cost and accuracy, we select one scan in the full-resolution branch as the default setting. Building upon the MS2D foundation, we introduce an SE block following EfficientVMamba [38], which further enhanced accuracy by 0.5% with minimal additional computational cost.

On ConvFFN. Upon replacing SS2D with MS2D and incorporating a SE block, we constructed a model that utilizes ConvFFN as a channel mixer. When only using SSM, the model exhibited insufficient information exchange between channels. The integration of ConvFFN as a channel mixer significantly enhanced the model’s capability for inter-channel information interaction. As indicated in Tab. 4, the addition of ConvFFN resulted in an additional accuracy improvement of 2.0%. To maintain a roughly equivalent computational cost, we adjusted the number of blocks within the model. Besides, we set the state space dimension $N = 1$ and stacked one more block to further enhance the capability of capturing long-range information while maintaining a roughly constant computational cost. This operation resulted in an additional accuracy improvement of 0.7%, as shown in Tab. 4.

Table 5: Ablation study on Multi-Scale 2D Scan.

Full	Half	#param	FLOPs	Top-1 Acc(%).
0	4	5.1M	0.74G	63.1
1	3	4.8M	0.89G	71.9
2	2	5.0M	1.00G	72.0
3	1	5.3M	1.11G	72.5
4	0	5.1M	1.19G	72.3

5 Limitations

The design of multi-scale VMamba aims to tackle the long-range forgetting problem of Mamba models with limited parameters on vision tasks. Although the proposed model has proven to be effective, its scalability remains to be explored since this issue can also be alleviated by increasing model sizes. In such cases, the multi-scale design may have only a marginal improvement.

6 Conclusion

In this paper, we introduced Multi-Scale VMamba (MSVMamba), an SSM-based vision backbone that leverages the advantages of linear complexity and global receptive field. We developed the Multi-Scale 2D (MS2D) scanning technique to minimize computational redundancy and alleviate the long-range forgetting problem in parameter-limited vision models. Additionally, we incorporated the Convolutional Feed-Forward Network (ConvFFN) to enhance the exchange of information between channels, thereby significantly improving the performance of our model. Our experiments demonstrate that MSVMamba consistently outperforms popular models from various architectures, including ConvNeXt, Swin Transformer, and VMamba, in image classification and downstream tasks.

References

- [1] Tianxiang Chen, Zhentao Tan, Tao Gong, Qi Chu, Yue Wu, Bin Liu, Jieping Ye, and Nenghai Yu. Mim-istd: Mamba-in-mamba for efficient infrared small target detection. *arXiv preprint arXiv:2403.02148*, 2024.
- [2] Zihang Dai, Hanxiao Liu, Quoc V Le, and Mingxing Tan. Coatnet: Marrying convolution and attention for all data sizes. *NeurIPS*, 2021.
- [3] Jia Deng, Wei Dong, Richard Socher, Li-Jia Li, Kai Li, and Li Fei-Fei. Imagenet: A large-scale hierarchical image database. In *CVPR*, 2009.
- [4] Xiaohan Ding, Xiangyu Zhang, Yizhuang Zhou, Jungong Han, Guiguang Ding, and Jian Sun. Scaling up your kernels to 31x31: Revisiting large kernel design in cnns. In *CVPR*, 2022.
- [5] Xiaoyi Dong, Jianmin Bao, Dongdong Chen, Weiming Zhang, Nenghai Yu, Lu Yuan, Dong Chen, and Baining Guo. Cswin transformer: A general vision transformer backbone with cross-shaped windows. In *CVPR*, 2022.
- [6] Alexey Dosovitskiy, Lucas Beyer, Alexander Kolesnikov, Dirk Weissenborn, Xiaohua Zhai, Thomas Unterthiner, Mostafa Dehghani, Matthias Minderer, Georg Heigold, Sylvain Gelly, et al. An image is worth 16x16 words: Transformers for image recognition at scale. In *ICLR*, 2020.
- [7] Chengbin Du, Yanxi Li, and Chang Xu. Understanding robustness of visual state space models for image classification. *arXiv preprint arXiv:2403.10935*, 2024.
- [8] Daniel Y Fu, Tri Dao, Khaled K Saab, Armin W Thomas, Atri Rudra, and Christopher Ré. Hungry hungry hippos: Towards language modeling with state space models. *arXiv preprint arXiv:2212.14052*, 2022.
- [9] Benjamin Graham, Alaaeldin El-Nouby, Hugo Touvron, Pierre Stock, Armand Joulin, Hervé Jégou, and Matthijs Douze. Levit: a vision transformer in convnet’s clothing for faster inference. In *ICCV*, 2021.
- [10] Albert Gu and Tri Dao. Mamba: Linear-time sequence modeling with selective state spaces. *arXiv preprint arXiv:2312.00752*, 2023.
- [11] Albert Gu, Tri Dao, Stefano Ermon, Atri Rudra, and Christopher Ré. Hippo: Recurrent memory with optimal polynomial projections. *NeurIPS*, 2020.
- [12] Albert Gu, Karan Goel, and Christopher Ré. Efficiently modeling long sequences with structured state spaces. *arXiv preprint arXiv:2111.00396*, 2021.
- [13] Albert Gu, Isys Johnson, Karan Goel, Khaled Saab, Tri Dao, Atri Rudra, and Christopher Ré. Combining recurrent, convolutional, and continuous-time models with linear state space layers. *NeurIPS*, 2021.
- [14] Hang Guo, Jinmin Li, Tao Dai, Zhihao Ouyang, Xudong Ren, and Shu-Tao Xia. Mambair: A simple baseline for image restoration with state-space model. *arXiv preprint arXiv:2402.15648*, 2024.
- [15] Jianyuan Guo, Kai Han, Han Wu, Yehui Tang, Xinghao Chen, Yunhe Wang, and Chang Xu. Cmt: Convolutional neural networks meet vision transformers. In *CVPR*, pages 12175–12185, 2022.
- [16] Kai Han, An Xiao, Enhua Wu, Jianyuan Guo, Chunjing Xu, and Yunhe Wang. Transformer in transformer. In *NeurIPS*, 2021.
- [17] Ali Hassani, Steven Walton, Jiachen Li, Shen Li, and Humphrey Shi. Neighborhood attention transformer. In *CVPR*, 2023.
- [18] Kaiming He, Georgia Gkioxari, Piotr Dollár, and Ross Girshick. Mask r-cnn. In *ICCV*, 2017.
- [19] Kaiming He, Xiangyu Zhang, Shaoqing Ren, and Jian Sun. Deep residual learning for image recognition. In *CVPR*, 2016.

- [20] Andrew G Howard, Menglong Zhu, Bo Chen, Dmitry Kalenichenko, Weijun Wang, Tobias Weyand, Marco Andreetto, and Hartwig Adam. Mobilenets: Efficient convolutional neural networks for mobile vision applications. *arXiv preprint arXiv:1704.04861*, 2017.
- [21] Jie Hu, Li Shen, and Gang Sun. Squeeze-and-excitation networks. In *CVPR*, 2018.
- [22] Gao Huang, Zhuang Liu, Geoff Pleiss, Laurens Van Der Maaten, and Kilian Weinberger. Convolutional networks with dense connectivity. *IEEE TPAMI*, 2019.
- [23] Tao Huang, Lang Huang, Shan You, Fei Wang, Chen Qian, and Chang Xu. Lightvit: Towards light-weight convolution-free vision transformers. *arXiv preprint arXiv:2207.05557*, 2022.
- [24] Tao Huang, Xiaohuan Pei, Shan You, Fei Wang, Chen Qian, and Chang Xu. Localmamba: Visual state space model with windowed selective scan. *arXiv preprint arXiv:2403.09338*, 2024.
- [25] Zihang Jiang, Qibin Hou, Li Yuan, Daquan Zhou, Xiaojie Jin, Anran Wang, and Jiashi Feng. Token labeling: Training a 85.5% top-1 accuracy vision transformer with 56m parameters on imagenet. *arXiv preprint arXiv:2104.10858*, 2021.
- [26] Alex Krizhevsky, Ilya Sutskever, and Geoffrey E Hinton. Imagenet classification with deep convolutional neural networks. *NeurIPS*, 2012.
- [27] Kunchang Li, Xinhao Li, Yi Wang, Yinan He, Yali Wang, Limin Wang, and Yu Qiao. Videomamba: State space model for efficient video understanding. *arXiv preprint arXiv:2403.06977*, 2024.
- [28] Weibin Liao, Yinghao Zhu, Xinyuan Wang, Cehngwei Pan, Yasha Wang, and Liantao Ma. Lightm-unet: Mamba assists in lightweight unet for medical image segmentation. *arXiv preprint arXiv:2403.05246*, 2024.
- [29] Tsung-Yi Lin, Michael Maire, Serge Belongie, James Hays, Pietro Perona, Deva Ramanan, Piotr Dollár, and C Lawrence Zitnick. Microsoft coco: Common objects in context. In *ECCV*, 2014.
- [30] Weifeng Lin, Ziheng Wu, Jiayu Chen, Jun Huang, and Lianwen Jin. Scale-aware modulation meet transformer. In *ICCV*, 2023.
- [31] Yue Liu, Yunjie Tian, Yuzhong Zhao, Hongtian Yu, Lingxi Xie, Yaowei Wang, Qixiang Ye, and Yunfan Liu. Vmamba: Visual state space model. *arXiv preprint arXiv:2401.10166*, 2024.
- [32] Ze Liu, Han Hu, Yutong Lin, Zhuliang Yao, Zhenda Xie, Yixuan Wei, Jia Ning, Yue Cao, Zheng Zhang, Li Dong, et al. Swin transformer v2: Scaling up capacity and resolution. In *CVPR*, 2022.
- [33] Ze Liu, Yutong Lin, Yue Cao, Han Hu, Yixuan Wei, Zheng Zhang, Stephen Lin, and Baining Guo. Swin transformer: Hierarchical vision transformer using shifted windows. In *ICCV*, 2021.
- [34] Zhuang Liu, Hanzi Mao, Chao-Yuan Wu, Christoph Feichtenhofer, Trevor Darrell, and Saining Xie. A convnet for the 2020s. In *CVPR*, 2022.
- [35] Jun Ma, Feifei Li, and Bo Wang. U-mamba: Enhancing long-range dependency for biomedical image segmentation. *arXiv preprint arXiv:2401.04722*, 2024.
- [36] Eric Nguyen, Karan Goel, Albert Gu, Gordon Downs, Preey Shah, Tri Dao, Stephen Baccus, and Christopher Ré. S4nd: Modeling images and videos as multidimensional signals with state spaces. *NeurIPS*, 2022.
- [37] Xuran Pan, Chunjiang Ge, Rui Lu, Shiji Song, Guanfu Chen, Zeyi Huang, and Gao Huang. On the integration of self-attention and convolution. In *CVPR*, 2022.
- [38] Xiaohuan Pei, Tao Huang, and Chang Xu. Efficientvmamba: Atrous selective scan for light weight visual mamba. *arXiv preprint arXiv:2403.09977*, 2024.
- [39] Ilija Radosavovic, Raj Prateek Kosaraju, Ross Girshick, Kaiming He, and Piotr Dollár. Designing network design spaces. In *CVPR*, 2020.

- [40] Jiacheng Ruan and Suncheng Xiang. Vm-unet: Vision mamba unet for medical image segmentation. *arXiv preprint arXiv:2402.02491*, 2024.
- [41] Karen Simonyan and Andrew Zisserman. Very deep convolutional networks for large-scale image recognition. *arXiv preprint arXiv:1409.1556*, 2014.
- [42] Jimmy TH Smith, Andrew Warrington, and Scott W Linderman. Simplified state space layers for sequence modeling. *arXiv preprint arXiv:2208.04933*, 2022.
- [43] Mingxing Tan and Quoc Le. Efficientnet: Rethinking model scaling for convolutional neural networks. In *ICML*, 2019.
- [44] Hugo Touvron, Matthieu Cord, Matthijs Douze, Francisco Massa, Alexandre Sablayrolles, and Hervé Jégou. Training data-efficient image transformers & distillation through attention. In *ICML*, 2021.
- [45] Hugo Touvron, Matthieu Cord, and Hervé Jégou. Deit iii: Revenge of the vit. In *ECCV*, 2022.
- [46] Hugo Touvron, Matthieu Cord, Alexandre Sablayrolles, Gabriel Synnaeve, and Hervé Jégou. Going deeper with image transformers. In *ICCV*, 2021.
- [47] Zhengzhong Tu, Hossein Talebi, Han Zhang, Feng Yang, Peyman Milanfar, Alan Bovik, and Yinxiao Li. Maxvit: Multi-axis vision transformer. In *ECCV*, 2022.
- [48] Ashish Vaswani, Noam Shazeer, Niki Parmar, Jakob Uszkoreit, Llion Jones, Aidan N Gomez, Łukasz Kaiser, and Illia Polosukhin. Attention is all you need. In *NeurIPS*, 2017.
- [49] A Wang, H Chen, Z Lin, H Pu, and G Ding. Repvit: Revisiting mobile cnn from vit perspective. *arxiv 2023*. *arXiv preprint arXiv:2307.09283*, 2023.
- [50] Wenhai Wang, Jifeng Dai, Zhe Chen, Zhenhang Huang, Zhiqi Li, Xizhou Zhu, Xiaowei Hu, Tong Lu, Lewei Lu, Hongsheng Li, et al. Internimage: Exploring large-scale vision foundation models with deformable convolutions. *arXiv preprint arXiv:2211.05778*, 2022.
- [51] Wenhai Wang, Enze Xie, Xiang Li, Deng-Ping Fan, Kaitao Song, Ding Liang, Tong Lu, Ping Luo, and Ling Shao. Pyramid vision transformer: A versatile backbone for dense prediction without convolutions. In *ICCV*, 2021.
- [52] Wenhai Wang, Enze Xie, Xiang Li, Deng-Ping Fan, Kaitao Song, Ding Liang, Tong Lu, Ping Luo, and Ling Shao. Pvt v2: Improved baselines with pyramid vision transformer. *Computational Visual Media*, 2022.
- [53] Zhuofan Xia, Xuran Pan, Shiji Song, Li Erran Li, and Gao Huang. Dat++: Spatially dynamic vision transformer with deformable attention. *arXiv preprint arXiv:2309.01430*, 2023.
- [54] Tete Xiao, Yingcheng Liu, Bolei Zhou, Yuning Jiang, and Jian Sun. Unified perceptual parsing for scene understanding. In *ECCV*, 2018.
- [55] Saining Xie, Ross Girshick, Piotr Dollár, Zhuowen Tu, and Kaiming He. Aggregated residual transformations for deep neural networks. In *CVPR*, 2017.
- [56] Chenhongyi Yang, Zehui Chen, Miguel Espinosa, Linus Ericsson, Zhenyu Wang, Jiaming Liu, and Elliot J Crowley. Plainmamba: Improving non-hierarchical mamba in visual recognition. *arXiv preprint arXiv:2403.17695*, 2024.
- [57] Yuhuan Yang, Chaofan Ma, Jiangchao Yao, Zhun Zhong, Ya Zhang, and Yanfeng Wang. Remamber: Referring image segmentation with mamba twister. *arXiv preprint arXiv:2403.17839*, 2024.
- [58] Weihao Yu, Mi Luo, Pan Zhou, Chenyang Si, Yichen Zhou, Xinchao Wang, Jiashi Feng, and Shuicheng Yan. Metaformer is actually what you need for vision. In *CVPR*, 2022.
- [59] Bolei Zhou, Hang Zhao, Xavier Puig, Sanja Fidler, Adela Barriuso, and Antonio Torralba. Scene parsing through ade20k dataset. In *CVPR*, 2017.

- [60] Lei Zhu, Xinjiang Wang, Zhanghan Ke, Wayne Zhang, and Rynson Lau. Biformer: Vision transformer with bi-level routing attention. In *CVPR*, 2023.
- [61] Lianghui Zhu, Bencheng Liao, Qian Zhang, Xinlong Wang, Wenyu Liu, and Xinggang Wang. Vision mamba: Efficient visual representation learning with bidirectional state space model. *arXiv preprint arXiv:2401.09417*, 2024.

Appendix

Throughput Comparison

We present the throughput comparison of our MSVMamba variants, and the baseline VMamba-Tiny on the ImageNet-1K dataset in Tab. 6. The throughput is measured in images per second, processed on a NVIDIA GeForce RTX 2080 Ti GPU. The image size for all tests is 224×224 , and the batch size is set to 128. Under similar GFLOPs, our MSVMamba-Tiny model nearly doubles the throughput of the baseline VMamba-Tiny.

Table 6: Throughput comparison on ImageNet-1K.

Model	Throughput (img/sec)
VMamba-Tiny	218.86
MSVMamba-Nano	1165.71
MSVMamba-Micro	887.14
MSVMamba-Tiny	421.80

Qualitative Analysis

We provide visualizations in Fig. 6 comparing the proposed MS2D and SS2D configurations in VMamba. These visualizations are generated by converting the S6 layer into an attention format, as demonstrated by VMamba [31]. The results clearly show that the full-resolution in MS2D scan captures more detailed features, whereas the scans at half resolution primarily focus on broader architectural details, compared to SS2D. The proposed hierarchical scanning pattern facilitates the current layer’s ability to discern and amalgamate features across various levels of abstraction.

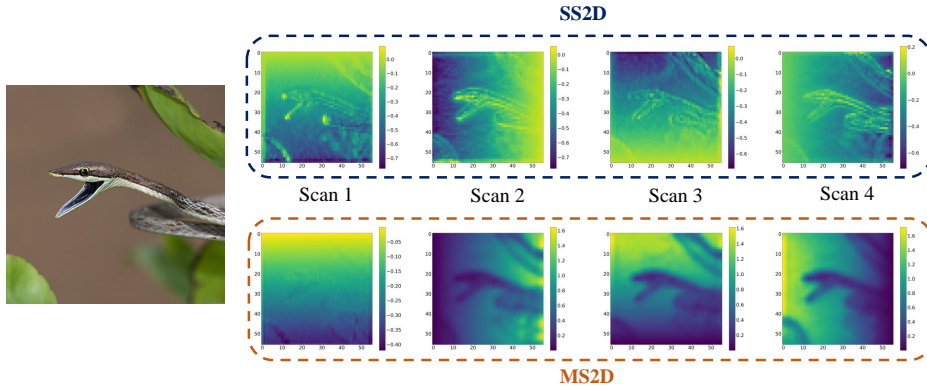


Figure 6: Attention maps from four distinct scanning directions, generated by SS2D and our MS2D in the last layer of the second stage. In the second row, full-resolution scan (first scan) captures fine-grained features, whereas scans at half resolution capture coarse-grained features. Maps are rendered at a higher resolution to enhance visualization quality.

Network Architecture

In Tab. 7, we present the detailed architecture of our model variants, including the Nano, Micro, and Tiny versions, each with varying channels and block numbers.

Table 7: Architectural overview of the MSVMamba series.

layer name	output size	Nano	Micro	Tiny
stem	56×56	conv 4×4 , 48, stride 4	conv 4×4 , 64, stride 4	conv 4×4 , 96, stride 4
stage 1	28×28	MS3 $\times 1$ conv 2×2 , 96, stride 2	MS3 $\times 1$ conv 2×2 , 128, stride 2	MS3 $\times 1$ conv 2×2 , 192, stride 2
stage 2	14×14	MS3 $\times 2$ conv 2×2 , 192, stride 2	MS3 $\times 2$ conv 2×2 , 256, stride 2	MS3 $\times 2$ conv 2×2 , 384, stride 2
stage 3	7×7	MS3 $\times 5$ conv 2×2 , 384, stride 2	MS3 $\times 5$ conv 2×2 , 512, stride 2	MS3 $\times 9$ conv 2×2 , 768, stride 2
stage 4	7×7	MS3 $\times 2$	MS3 $\times 2$	MS3 $\times 2$
	1×1	average pool, 1000-d fc, softmax		
Param. (M)		6.9	11.9	33.0
FLOPs		0.9×10^9	1.5×10^9	4.6×10^9